JVI Journals.ASM.org

In Vivo Bioluminescent Imaging of Influenza A Virus Infection and Characterization of Novel Cross-Protective Monoclonal Antibodies

Nicholas S. Heaton, Victor H. Leyva-Grado, Gene S. Tan, Dirk Eggink, Rong Hai, Peter Palese

Icahn School of Medicine at Mount Sinai, Department of Microbiology, New York, New York, USA

Influenza A virus is a major human pathogen responsible for seasonal epidemics as well as pandemic outbreaks. Due to the continuing burden on human health, the need for new tools to study influenza virus pathogenesis as well as to evaluate new therapeutics is paramount. We report the development of a stable, replication-competent luciferase reporter influenza A virus that can be used for *in vivo* imaging of viral replication. This imaging is noninvasive and allows for the longitudinal monitoring of infection in living animals. We used this tool to characterize novel monoclonal antibodies that bind the conserved stalk domain of the viral hemagglutinin of H1 and H5 subtypes and protect mice from lethal disease. The use of luciferase reporter influenza viruses allows for new mechanistic studies to expand our knowledge of virus-induced disease and provides a new quantitative method to evaluate future antiviral therapies.

Influenza A virus (IAV) is a major cause of respiratory infection in humans and is associated with significant morbidity and mortality worldwide every year (1). Furthermore, the segmented nature of the genome imparts the ability for reassortment between human, avian, and/or swine strains, which can lead to new pandemic strains of influenza virus that continue to pose major human health risks (2). Much work has been done investigating the mechanisms of IAV pathogenesis (3, 4); monitoring viral infection and spread in real time and in living animals, however, has remained elusive.

In other disease models, the introduction of luciferase reporter genes directly into tumor tissue or pathogen has been shown to be an effective method for monitoring disease (5–8). Having an integrated reporter gene not only allows for rapid quantification of viral replication levels but also, upon introduction of the luciferase substrate, permits noninvasive imaging of infected tissues (9). Dynamic whole-body imaging of living animals allows for assessing not only where in the body the infection starts but also where it spreads. This is especially important for influenza A virus infection since the replication sites of different strains of the virus in the respiratory tract can be influenced by the preference for receptors with sialic acid α2,3 or α2,6 linkages (10–12). Further, many highly virulent strains such as highly pathogenic avian influenza (H5N1) virus can spread to the central nervous system (13), which likely exacerbates disease severity (14). Currently, there is a lack of methods to study these aspects of pathogenesis that do not involve euthanizing the infected animal. Further, with respect to therapeutic intervention, it is difficult to assess the efficacy of treatment on reducing viral replication or tissue spread in living animals.

In this report, we describe the generation of a stable, fully infectious influenza A virus which encodes a luciferase reporter protein in a novel insertion site. We use this virus to establish a noninvasive method for whole-body imaging of virus infection and spread in real time. Additionally, we use this virus to evaluate novel therapeutic monoclonal antibodies (MAbs) which neutralize both H1 and H5 subtype viruses. This study not only represents the first report of noninvasive imaging of influenza virus infection but also provides a platform for further pathogenesis and therapeutic efficacy studies.

MATERIALS AND METHODS

Cell culture. Madin-Darby canine kidney (MDCK) cells and 293T cells were maintained in Dulbecco's minimum essential medium (DMEM) containing 10% fetal bovine serum and penicillin-streptomycin.

Plasmids and generation of recombinant viruses. Plasmids encoding PB2-GLuc (where GLuc is *Gaussia* luciferase) were generated in the pDZ vector, which expresses both viral protein and viral RNA (vRNA) for virus rescue as previously described (15). The PB2 open reading frame (ORF) was amplified from a construct in which the packaging signals in the ORF were silently mutated and duplicated between the ORF and the untranslated region (UTR) as previously described (16, 17). The primers For (5′-GGAAGACAGGAGAAGAAGCTAGCCATGGAGCGGATCAAGGAG-3′) and Rev (5′-GGGCCCGGGGTTGGACTCGACG-3′) were used. The foot-and-mouth disease virus (FMDV) 2A sequence (QLLNFDLLKLAGDVESNPGP) was introduced by annealing oligonucleotide encoding the sequence and overlapping the PB2 and GLuc ORFs to allow recombination, using the following primers: For, 5′-GCTGCCGCGCAGCTGTTGAATTTTGACCTTCTTAAGCTTGCGGGAGACGTCGAGTCCAACCCCGGGCCC-3′; Rev, 5′-GGGCCCGGGGTTGGACTCGACGTCTCCCGCAAGCTTAAGAAGGTCAAAATTCAACAGCTGCGCGGCAGC-3′. The GLuc ORF was amplified from a humanized GLuc plasmid (NEB) with the KDEL motif encoded in the reverse primer, as follows: For, 5′-GTCCAACCCCGGGCCCATGGGAGTCAAAGTTCTG-3′; Rev, 5′-CCTTCTCTCCTTTCTCGAGCTACAGTTCGTCTTTGTCACCACCGGCCCCCTT-3′. The complete construct was generated by Infusion HD (Clontech) recombination of the pDZ vector, the PB2 ORF, and the GLuc ORF. To remove the duplicated packaging signals at the 5′ end of the PB2 ORF, wild-type (WT) and PB2-GLuc constructs were digested with SacI and BsrGI, and the mutant 5′ end was replaced with the wild type. This left a single duplicated packaging signal consisting of 129 nucleotides (nt) on the 3′ end. All constructs were fully sequenced. The recombinant PB2 was introduced into 293T cells via Lipofectamine 2000 (Invitrogen) transfection along with the seven WT plasmids encoding the other viral segments, as previously de-

Received 9 April 2013 Accepted 14 May 2013
Published ahead of print 22 May 2013
Address correspondence to Peter Palese, peter.palese@mssm.edu.

doi:10.1128/JVI.00969-13

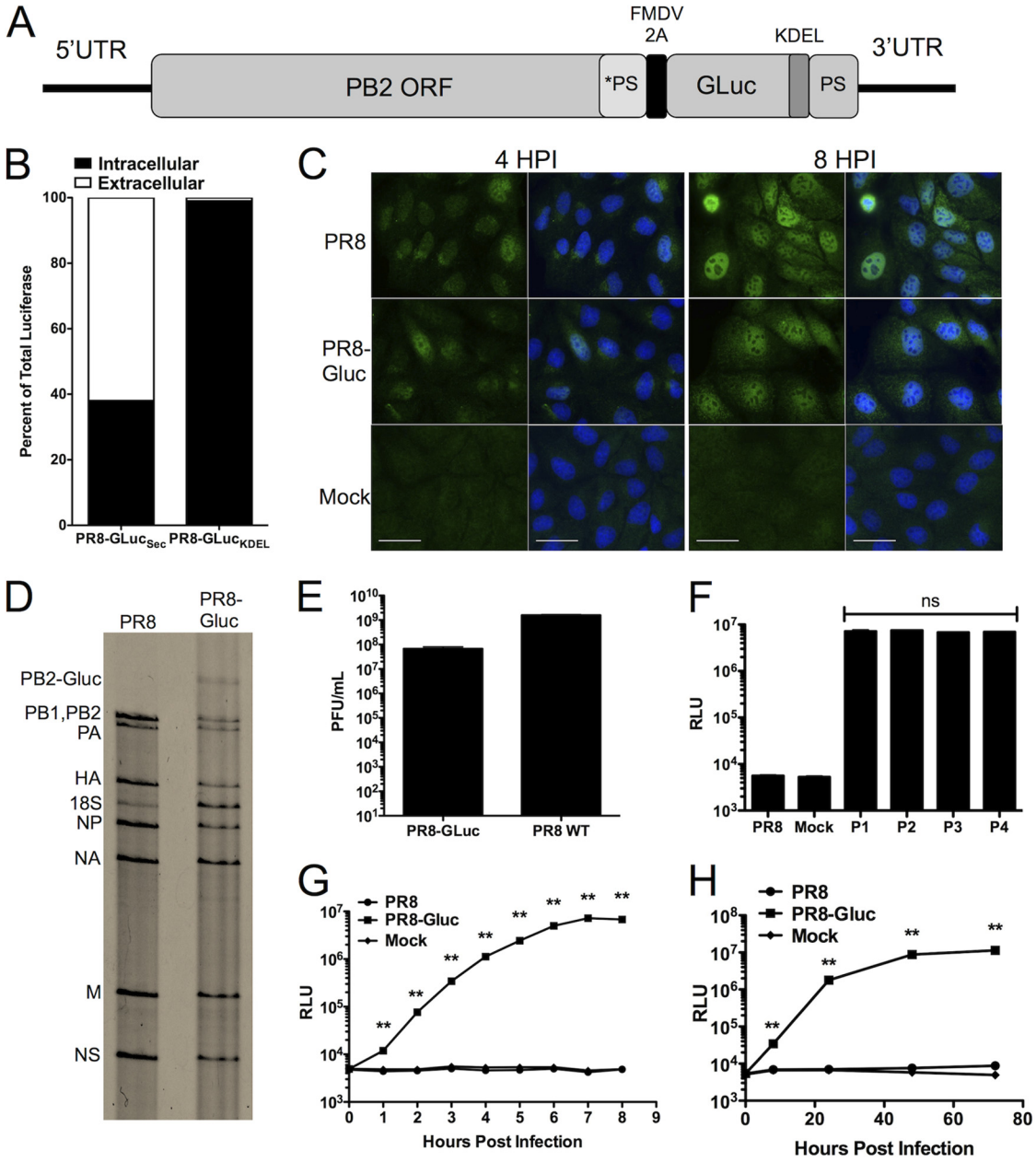

FIG 1 *In vitro* characterization of PR8-GLuc. (A) Schematic representation of the PB2 segment encoding the GLuc transgene. *PS represents silent mutations of the original packaging signal; PS represents the duplicated original packaging sequence. (B) MDCK cells were infected with PR8-GLuc with and without a KDEL ER retention signal. The relative percentages of secreted and intracellular GLuc signals are shown. (C) MDCK cells were infected with WT PR8 or PR8-GLuc at an MOI of 1 and fixed at the indicated times. PB2 cellular localization was probed with an anti-PB2 antibody. Scale bar, 20 μm. (D) Viral RNA was extracted from either WT PR8 or PR8-GLuc virions and resolved on a polyacrylamide gel. RNA was stained via silver stain. 18S represents rRNA contamination of the virion preparation. (E) Titers in PFU/ml of WT PR8 and PR8-GLuc after 48 h of growth in eggs at 37°C. (F) MDCK cells were mock infected or infected with WT PR8 or with PR8-GLuc from serial passage experiments in eggs (passages 1 to 4) at an MOI of 1. At 6 hpi cells were harvested, and luciferase assays were performed. (G) MDCK cells were mock or virus infected at an MOI of 1 and incubated without TPCK-trypsin for the indicated time points. At the indicated times, luciferase activity was determined. (H) MDCK cells were mock or virus infected at an MOI of 0.001 and incubated with TPCK-trypsin for the indicated times. Cellular lysates were collected, and luciferase activity was determined. **, $P \leq 0.001$; ns, not significant. NA, neuraminidase; RLU, relative light units.

scribed (18). Rescued virus was amplified in 10-day-old embryonated chicken eggs (Charles River) at 37°C for 48 h.

***In vitro* growth curves.** MDCK cells were infected at the multiplicities of infection (MOIs) indicated in the legend to Fig. 1. For single-cycle growth curves, cells were incubated in DMEM without tosylsulfonyl phenylalanyl chloromethyl ketone (TPCK)-trypsin. At the times indicated in Fig. 1, cells were lysed, and luciferase assays were performed. For multicycle growth curves, MDCK cells were infected and incubated with TPCK-trypsin to allow virus spread. At the times indicated in Fig. 1, the cells were lysed, and luciferase assays were performed to assay viral replication.

vRNA gel. Virus was amplified in 10-day-old embryonated chicken eggs for 48 h. Forty milliliters of viral stocks was concentrated by spinning at 25,000 rpm in an ultracentrifuge (SW-28 rotor; Beckman) for 2 h over

a 30% sucrose cushion and resuspended in 200 μl of phosphate-buffered saline (PBS). Viral RNA was collected via TRIzol according to the manufacturer's instructions (Invitrogen). Two micrograms of RNA was resolved on a 2.8% polyacrylamide gel. vRNA was visualized by silver stain according to the manufacturer's instructions (Invitrogen).

Immunofluorescent staining and microscopy. For PB2 immunostaining, MDCK cells were infected at an MOI of 1. Four and eight hours postinfection, cells were fixed via a 10-min incubation with 4% paraformaldehyde in PBS. Cells were subsequently washed in PBS and permeabilized with 0.2% Triton in PBS for 30 min at room temperature. Cells were blocked overnight at 4°C in 5% bovine serum albumin (BSA) in PBS. Primary anti-PB2 monoclonal antibody (kindly provided by Chris Seibert) was incubated overnight at 4°C in 5% BSA in PBS. After three PBS washes, secondary antibody (donkey anti-mouse Alexa-Fluor 488; Invitrogen) was incubated with the cells for 1 h at room temperature. Cells were washed and mounted with ProLong Gold with 4′,6′-diamidino-2-phenylindole (DAPI; Invitrogen). Images were captured on and Olympus IX-70 camera. For immunofluorescence of monoclonal antibodies, MDCK cells were infected at an MOI of 5 with the viruses indicated in Fig. 4A. Cells were fixed with 0.5% paraformaldehyde in PBS. After samples were blocked in 5% milk, antibodies were diluted to 5 μg/ml and incubated with the cells for 1 h at room temperature (RT). After three PBS washes, secondary antibody (donkey anti-mouse Alexa-Fluor 488 Invitrogen) was incubated with cells for 1 h at RT. Fluorescence was visualized using an IX-70 inverted microscope (Olympus).

Luciferase assays and virus quantification. Luciferase assays were performed with a BioLux *Gaussia* Luciferase Assay Kit (NEB) according to the manufacturer's instructions. In cell culture, cells were lysed via Luciferase Cell Lysis Buffer (NEB), and 20 μl of cell lysate was assayed with 50 μl of luciferase substrate. For animal samples, 20 μl of lung homogenate was added to 50 μl of luciferase substrate. To quantify virus, samples were serially diluted in PBS and used to infect confluent monolayers of MDCK cells. After a 1-h incubation at 37°C, virus was removed, and a TPCK-trypsin-containing DMEM agar overlay was applied to the cells. At 48 h postinfection (hpi), agar was removed, and plaques were visualized by immunostaining with polyclonal serum from influenza A/Puerto Rico/8/1934 (PR8) virus as described in Bouvier et al. (19).

Antibody generation and characterization. Monoclonal antibodies were generated after immunization of mice as previously described (20). Enzyme-linked immunosorbent assays (ELISAs) showing hemagglutinin (HA)/antibody and viral plaque reduction assays were also performed as previously described (20).

***In vivo* imaging.** Infected animals were anesthetized via 2.5% isoflurane inhalation. Stocks of coelenterazine (5 mg/ml in 2% 3 M HCl in ethanol; Nanolight Technologies) were diluted in PBS before injection, and 100 μg of coelenterazine was injected in a total volume of 150 μl intravenously in the retro-orbital plexus. Exactly 20 s after injection, mice were imaged for 45 s via an IVIS Spectrum *in vivo* imaging system (PerkinElmer). All images were processed with the system software using the same threshold applied to the images across an experimental group.

Animal treatment experiments. Six- to eight-week-old BALB/c or DBA/2 mice (Jackson laboratories) were used for all of the experiments. For infection, mice were put under anesthesia using a mix of ketamine-xylazine (100/10 mg/kg), and the appropriate dose of the virus in a volume of 40 μl was administered intranasally. Animals were monitored daily, and body weights were recorded for 14 days. A weight loss of more than 25% of the original (day 0) body weight was considered the humane endpoint. When tissues were collected for analysis, samples were homogenized (Fastprep-24; MP Biomedicals) and spun at 10,000 rpm for 10 min; supernatants were collected and frozen at −80°C until used. For treatment, the antibodies were diluted to a concentration of 5 mg/kg and injected intraperitoneally (i.p.) 2 h before virus infection; the oseltamivir group received 5 mg/kg twice a day (b.i.d.) for 3 days starting 12 h before virus infection. All animal protocols were approved by the IACUC of the Icahn School of Medicine at Mount Sinai.

Statistical analysis. Unless otherwise stated, statistical significance was determined using an unpaired, two-tailed Student's *t* test. In cases where a sample was below the limit of detection, we assigned a value equal to the limit of detection.

RESULTS

To generate a luciferase reporter influenza A virus, we inserted the luciferase reporter gene into the IAV genome in the polymerase PB2 segment at the C terminus of the viral protein. This design was based on previous work that has shown that this location tolerates small tags (21). There are several obstacles in designing influenza A virus encoding a reporter protein. First, the virus segments are relatively small and do not tolerate large insertions well; second, the addition of a C-terminal tag to a viral protein will disrupt the packaging signals needed to assemble progeny virions. To address these concerns, we used *Gaussia* luciferase (GLuc), which is a relatively small luminescent protein (~20 kDa) but one which has a higher quantum yield than the more common *Renilla* or firefly luciferase (22). To restore packaging, we made silent mutations in the PB2 open reading frame (ORF) to eliminate the original packaging signals and then added the complete packaging signal after the GLuc insertion preceding the 3′ UTR. We tested various lengths of packaging signals; however, we observed that anything less than 120 nt significantly compromised the virus (data not shown). Finally, we separated the PB2 and GLuc ORFs with an FMDV 2A site, which cleaves the two proteins cotranslationally (23) (Fig. 1A).

We rescued the PB2-GLuc segment in the influenza A/Puerto Rico/8/1934 (PR8) H1N1 virus background. Since GLuc is a naturally secreted protein, we added a C-terminal endoplasmic reticulum (ER) retention sequence (KDEL) to prevent secretion (24). Upon infection of cells, the presence of a KDEL motif leads to a retention of more than 99% of the luciferase signal inside the cells, compared to less than 40% in its absence (Fig. 1B). In order to determine if expressing the GLuc protein from the PB2 segment influenced PB2 localization, we infected cells with either the parental PR8 strain or the luciferase virus, here referred to as PR8-GLuc. At 4 and 8 hpi, we observed no major differences in the signal or localization of the viral PB2 protein (Fig. 1C).

As a validation that the PR8-GLuc virus was harboring the transgene, we extracted RNA from PR8 and PR8-GLuc virions and resolved the segments on a polyacrylamide gel (Fig. 1D). We observed seven distinct viral RNA bands in the PR8 lane, six individual viral segments and one band corresponding to the PB1 and PB2 segments, which are the same size. However, in the PR8-GLuc lane, we observed eight bands and a loss of intensity from the PB1-PB2 band since the PB2 segment had been shifted due to the presence of the luciferase coding sequence. We grew purified clonal stocks of PR8-GLuc in eggs for use in subsequent studies. Upon titration of the amount of infectious particles after 48 h of growth in eggs, we observed a titer of approximately 1×10^8 PFU/ml; this is a 1 $\log_{10}$ reduction in titer compared to that of the WT PR8 (Fig. 1E).

Stability of a transgene in an RNA virus is a notoriously difficult feature to obtain (25–29). To determine the stability of GLuc in the PB2 segment, we performed serial passage experiments in eggs. After each passage, the virus was collected and then diluted at least 10^{-6} and then used to inoculate another egg, for a total of four passages. Virus from each passage was used to infect MDCK cells at an MOI of 1, and luciferase assays were performed (Fig.

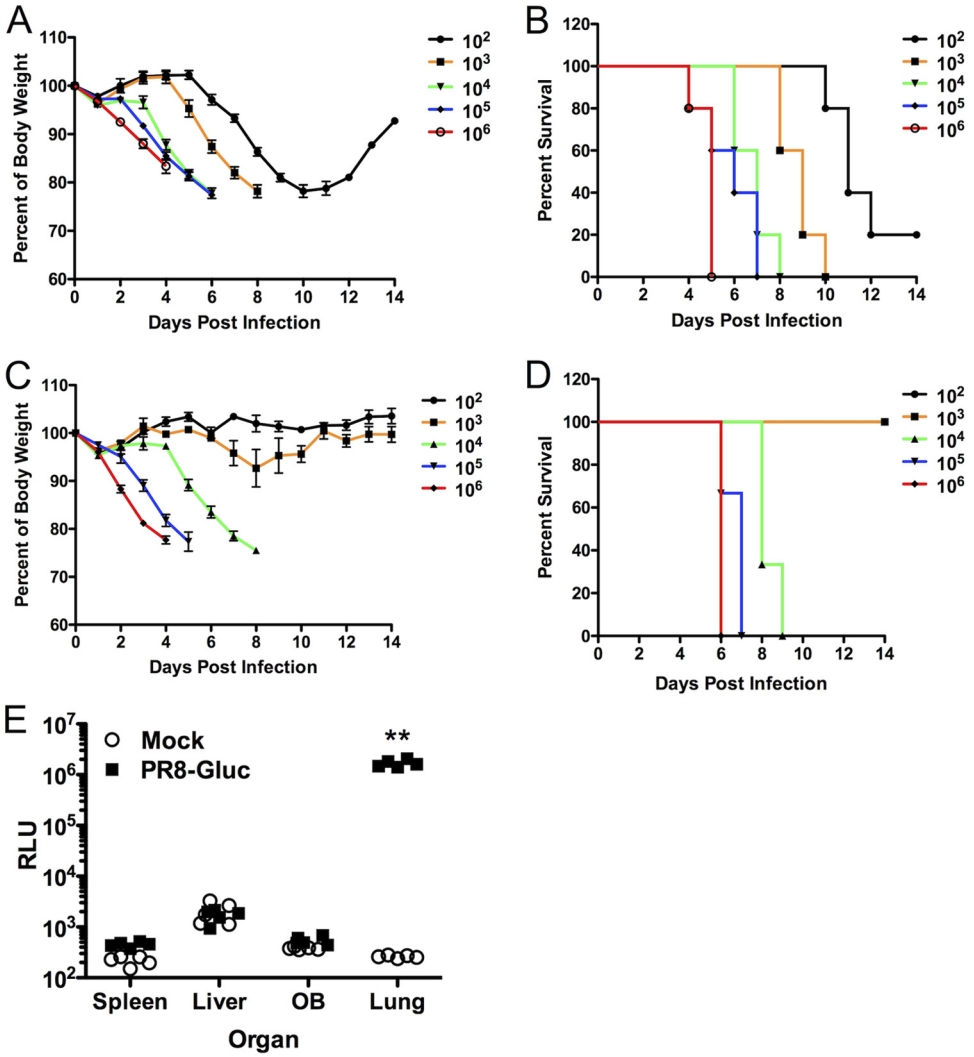

FIG 2 PR8-GLuc infection induces lethal disease in mice and exhibits the expected tropisms. (A and B) DBA/2 mice were infected with the indicated inoculum of PR8-GLuc and monitored for weight loss and lethality. (C and D) BALB/c mice were infected with the indicated inoculum of PR8-GLuc and monitored for weight loss and lethality. (E) DBA/2 mice were infected with 10^3 PFU of PR8-GLuc or mock infected. Three days after infection, the indicated organs were collected, and the levels of luciferase in these organs were determined (**, $P \leq 0.001$). OB, olfactory bulb.

1F). We observed no loss of luciferase signal upon virus passaging, suggesting that the luciferase gene was functionally maintained. Additionally, we purified vRNA from the four passages and amplified the PB2 segment via reverse transcription-PCR (RT-PCR). Virus was sequenced, and no mutations were present in the inserted sequences, showing that this insertion appears to be stable at least over four passages in eggs.

We next characterized the expression of the luciferase reporter over single and multicycle growth periods of PR8-GLuc in MDCK cells (Fig. 1G and H). In single-cycle growth (MOI of 1), the luciferase signal increases with time and plateaus by 7 to 8 hpi. There was no signal above background after infection with the parental PR8-infected control (Fig. 1G). In multicycle growth (MOI of 0.001), we observed the luciferase signal from PR8-GLuc to increase over 72 h, at which time we began to see cell death (Fig. 1H).

To further characterize PR8-GLuc, we infected two strains of mice, BALB/c and DBA/2, to represent relatively resistant and susceptible mouse genetic backgrounds, respectively (30, 31) (Fig. 2A to D). We observed weight loss and mortality in both backgrounds. The median lethal dose (LD_{50}) of virus for DBA/2 mice was ~60 PFU (Fig. 2A and B), and for BALB/c mice, the LD_{50} was calculated to be ~5,000 PFU (Fig. 2C and D). The LD_{50} for WT PR8 in BALB/c mice is between 50 and 100 PFU, so the PR8-GLuc virus LD_{50} is increased by 50 to 100 times, which is comparable to another published infectious reporter IAV which harbors green fluorescent protein (GFP) (32). We chose to use the DBA/2 mice for the remainder of the experiments, unless specifically noted otherwise, as they were significantly more susceptible to the virus.

IAV infection is an acute infection of the respiratory tract; we therefore collected tissues from infected mice and assayed for the presence of luciferase from infected animals to ensure that PR8-GLuc exhibited the expected tropism. As expected, the lungs displayed a significant increase, approximately 7,000-fold, in luciferase signal, which is highly statistically significant (Fig. 2E).

In order to visualize IAV infection in living animals, we in-

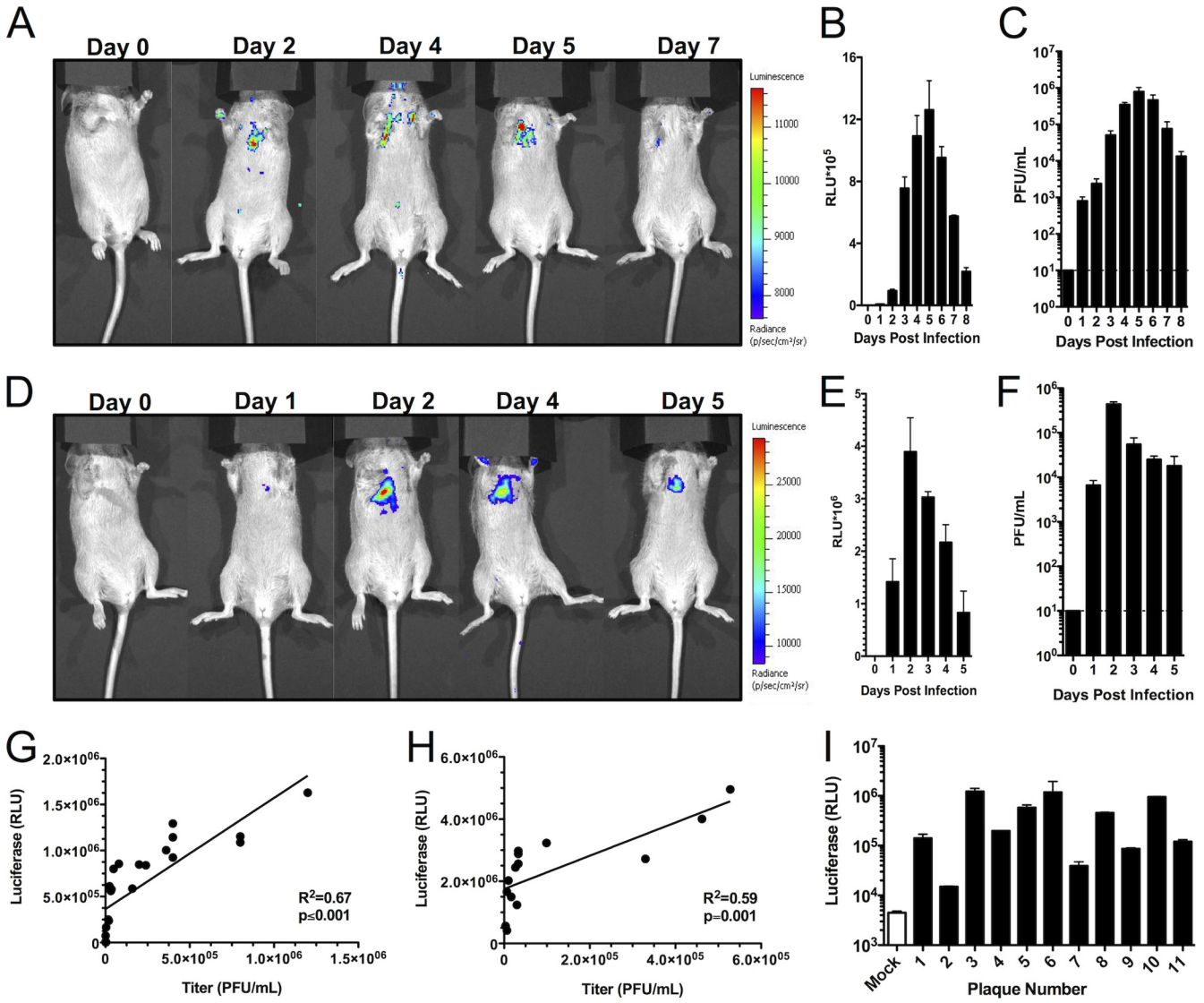

FIG 3 PR8-GLuc infection allows for *in vivo* imaging. Mice were infected with 10^3 PFU (A) or 10^5 PFU (D) and imaged at the indicated days. At the indicated times, lungs were collected from infected animals, and the amounts of luciferase and viral titers were determined. (B and C) Data correspond to the time course for the dose of 10^3 PFU. (E and F) Data correspond to the time course for the dose of 10^5 PFU. (G and H) Luciferase levels and viral titers from individual animals were plotted against each other from time courses of doses of 10^3 PFU(G) and 10^5 PFU (H). The R^2 and P values for the linear regression analyses are indicated on each graph. (I) Lung homogenates from animals at the day 4 time point (inoculum, 10^5 PFU) were plaque purified. Virus was isolated from each plaque and used to infect MDCK cells for 16 h. Cellular lysates were collected and subjected to luciferase assays. The white bar indicates mock-infected controls, and each black bar indicates the average luciferase value for an individual plaque-purified viral clone.

fected mice with two doses of PR8-GLuc (10^3 and 10^5 PFU) and monitored the luciferase signal over time via an IVIS Spectrum imager (Fig. 3A and D). While no signal was detected in mice before infection (day 0), we observed luciferase signals from the lungs at the earliest time point measured, 24 hpi. For the infections with 10^3 PFU, the virus replicates until the signal peaks around day 4 to 5 (Fig. 3A). With the higher dose (10^5 PFU), infection peaks earlier and starts declining after day 2 (Fig. 3D). At each day during the time course, animals were euthanized, and the luciferase levels and viral titers from lung homogenates were determined (Fig. 3B, C, E, and F). As expected, we observed animals that showed high signal levels during imaging to also have high viral titers and luciferase levels in lung homogenates. To formally test the correlation between the luciferase readings and titers from the lungs, we plotted the two variables against each other and performed a linear regression analysis (Fig. 3G and H). For time courses of both the dose of 10^3 PFU (Fig. 3G) and the dose of 10^5 PFU (Fig. 3H), we observed a statistically significant ($P \leq 0.001$) nonzero slope of the trend lines for the plots of these two variables.

To assess the stability of the luciferase reporter in animals over the length of the time course, we took lung homogenates from three animals from the day 4 time point (10^5 PFU inoculation) and plaque purified the virus. We isolated 11 viral clones from the plaques, infected MDCK cells for 16 h, and assayed for luciferase production. The MOI used to infect the MDCK cells varied by the size of the plaque isolated (leading to a range of luciferase values); however, in all cases the MOI was less than 1. All 11 clones were positive for luciferase (Fig. 3I). We have repeated this experiment and found even at 7 days

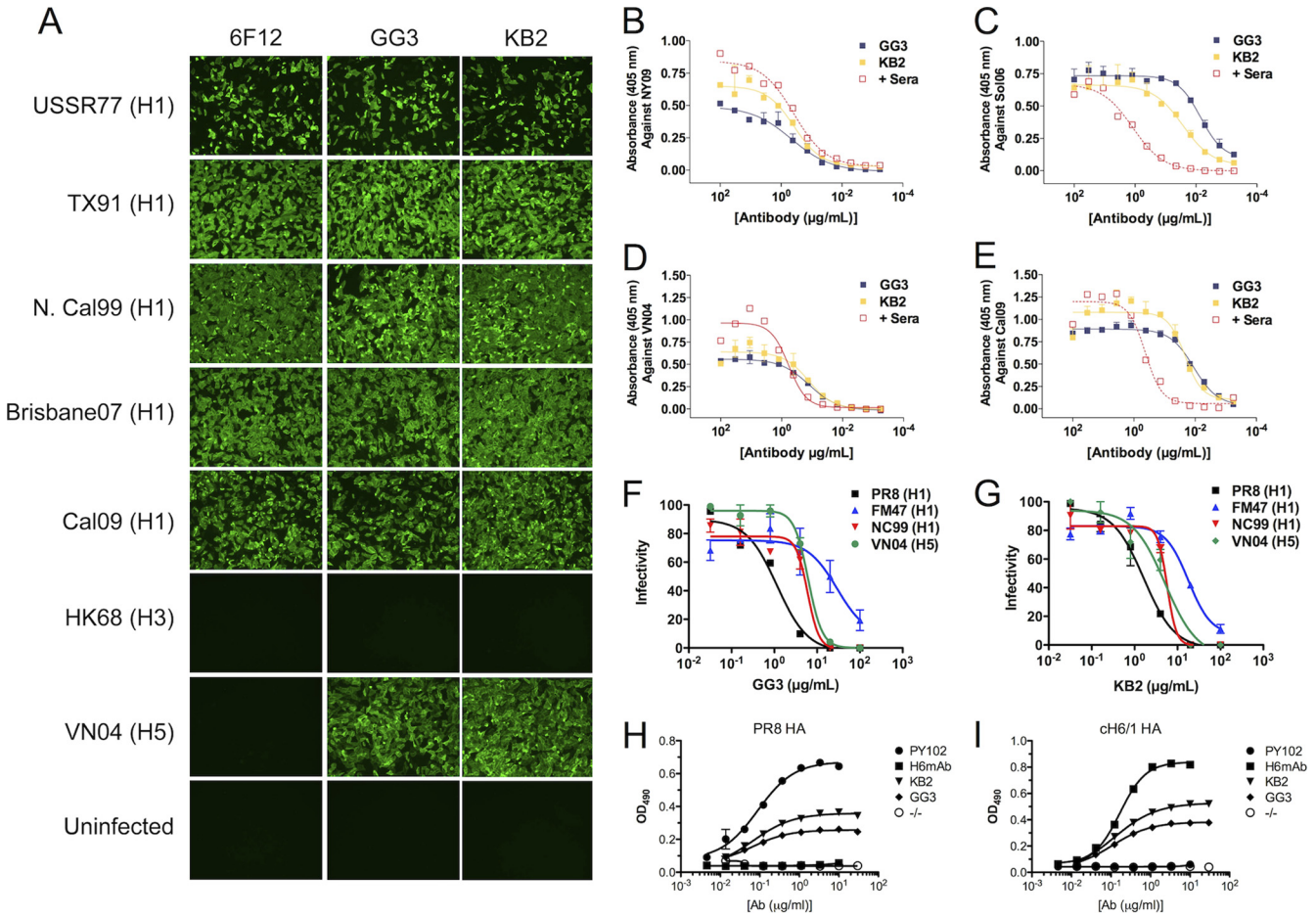

FIG 4 Novel monoclonal antibodies against the HA stalk region restrict a panel of H1 and H5 viruses. (A) Monoclonal antibodies GG3 and KB2 bind to HA on the surface of infected cells from all tested influenza A H1 virus strains, similar to the previously published pan-H1 antibody 6F12. GG3 and KB2, however, also bind an H5 avian isolate. None of the tested antibodies bound to H3 isolates. (B to E) Monoclonal antibodies GG3 and KB2 were incubated with hemagglutinin from the indicated viruses (as noted on the *y* axes) expressed and purified via a baculovirus expression system. Plates were coated with the purified protein, and reactivity of GG3 or KB2 via ELISA was determined. Positive (+) sera, polyclonal sera from convalescent mice infected with the appropriate viruses. (F and G) GG3 and KB2 were incubated with the indicated viruses in a plaque reduction assay. (H and I) ELISA plates were coated with hemagglutinin from the H1 PR8 virus or a chimeric HA protein consisting of an H6 head with the group 1 stalk from PR8 (cH6/1). The following antibodies were tested for reactivity against those proteins: PY102 (an H1 head-specific antibody), H6mAb (an antibody specific for H6 head domains), KB2, GG3, and a negative control. Viruses are abbreviated as follows: NY09, influenza A/NewYork/18/2009; Sol06, influenza/A/Solomon Islands/03/2006; VN04, influenza A/Vietnam/1203/2004 (H5N1); Cal09, influenza A/California/04/2009; USSR77, influenza A/USSR/77; TX91, influenza A/Texas/36/91; Brisbane07, influenza A/Brisbane/59/2007; HK68, influenza A/Hong Kong/1/1968; FM47, influenza A/Fort Monmouth/1/1947; N. Cal99 or NC99, influenza A/NewCaledonia/20/1999. Ab, antibody; OD_{490}, optical density at 490 nm.

postinfection that all tested viruses retained luciferase expression (data not shown). These experiments provide evidence that the luciferase reporter in PR8-GLuc is stable not only *in vitro* but also over multiple-day time courses in animals.

We decided to focus on using PR8-GLuc as a tool to evaluate the efficacy of antiviral therapeutics. As a preliminary experiment, we infected mice with PR8-GLuc and treated them with either the neuraminidase inhibitor oseltamivir, a previously published anti-influenza virus monoclonal antibody, 6F12 (20), or PBS as a control. We then imaged the infected animals daily over a 3-day time course. We observed a major difference in the luciferase signals from the lungs between PBS-treated mice and other treatment groups, with the largest differences apparent 3 to 4 days postinfection (data not shown). This experiment provided proof of principle that PR8-GLuc is capable of acting as a metric for therapeutic efficacy.

We expanded upon our preliminary studies and next used PR8-GLuc to characterize the therapeutic potential of novel anti-IAV monoclonal antibodies. A major interest in the IAV field is the characterization of antibodies which bind a conserved region of the IAV hemagglutinin (HA) glycoprotein, termed the "stalk" domain. This domain is much less variable than the "head" region, and therapeutics targeting this domain potentially have the ability to cross-protect against multiple variants and subtypes of IAV (33). To evaluate the therapeutic potential of stalk antibodies, our group has generated monoclonal antibodies that bind this region (20, 34). Hybridomas from immunized mice were screened by determining their reactivity against IAV HA. We identified two monoclonal antibodies, GG3 and KB2 (18), which showed a high degree of binding not only to a range of H1 viruses (similar to our previously published 6F12 antibody [20]) but also to H5 HA on the surface of infected cells (Fig. 4A) and in purified HA ELISAs (Fig. 4B to E). These antibodies also have strong neutralization activities in plaque reduction assays against multiple strains of IAV (Fig. 4F and G).

Despite strong HA binding and inhibition of viral plaque for-

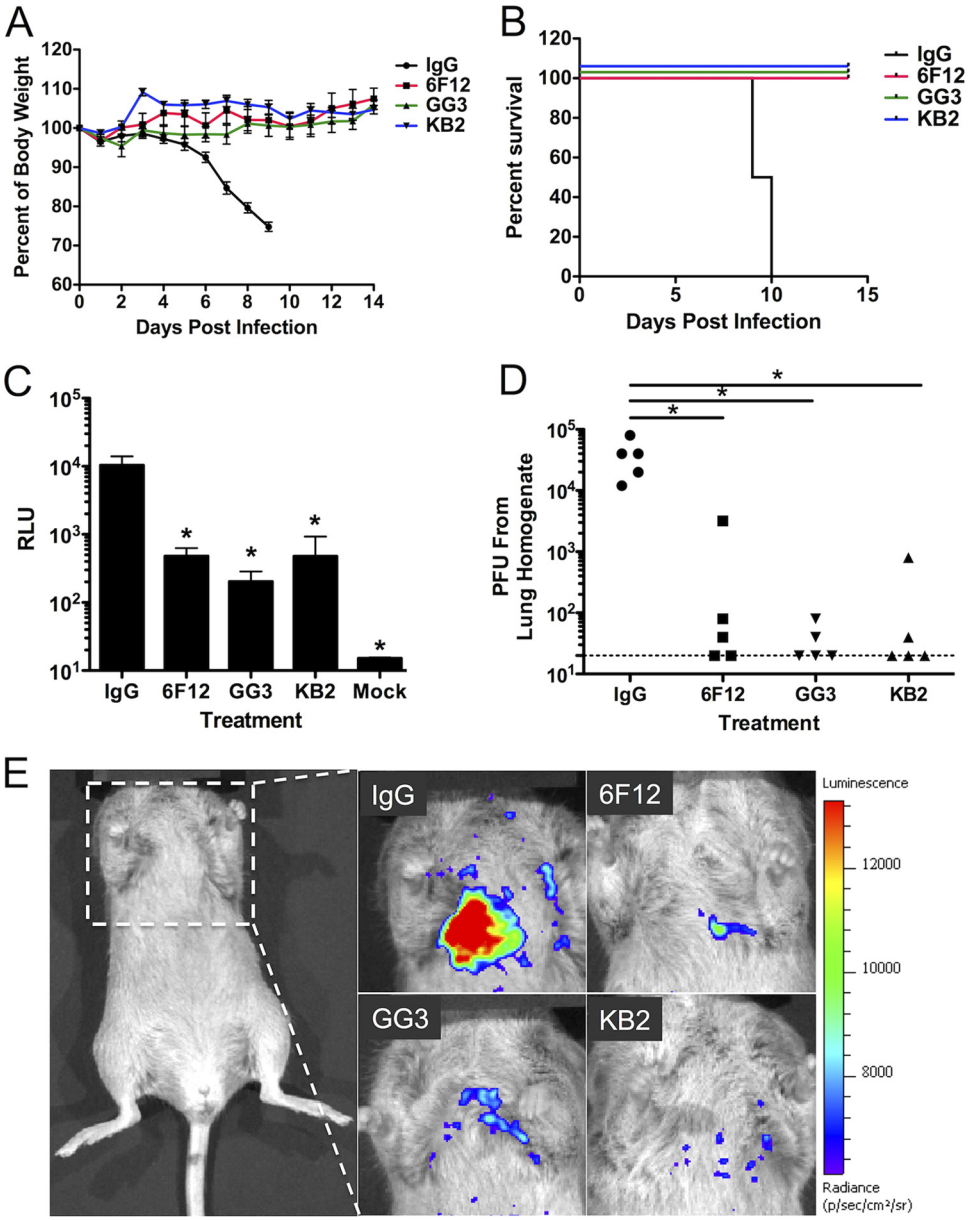

FIG 5 GG3 and KB2 restrict PR8-GLuc replication *in vivo*. (A and B) DBA/2 mice were treated i.p. with 5 mg/kg of the indicated antibodies or an isotype control at 2 h preinfection. Mice were then challenged with 5 LD_{50}s of PR8-GLuc and monitored over time for weight loss and survival. (C and D) Lungs from mice infected as described for panels A and B were collected 5 days postinfection and assayed for luciferase levels (C) and viral titers (D). The dotted line in panel D indicates the limit of detection. *, $P \leq 0.05$. (E) Mice infected as described for panels A and B were imaged at 5 days postinfection to determine virus replication.

mation, these antibodies are negative in a hemagglutination inhibition assay. This is characteristic of antibodies which bind the HA stalk domain. Although it is unlikely that our monoclonal antibodies would bind an epitope common to the head domain of both H5 and H1 viruses and still allow hemagglutination activity, we performed ELISAs with a chimeric HA protein (18) consisting of an H6 head and an H1 stalk. We observed robust binding of GG3 and KB2 to this protein while head-specific antibodies lost binding (Fig. 4H and I); this is indicative of stalk binding.

Since these antibodies showed neutralization activity *in vitro*, we performed passive transfer experiments of DBA/2 mice with GG3 and KB2 and with 6F12 as a positive control and 22A6 (isotype MAb negative control). Mice were given a 5-mg/kg dose 2 h before infection and were then challenged with 5 LD_{50} of PR8-GLuc. We observed no morbidity or mortality of mice receiving the antibody therapies while the isotype control-treated mice all succumbed to disease by day 10 postinfection (Fig. 5A and B). In parallel, at day 5 postinfection, we also imaged mice and collected lungs to quantify luciferase activity and viral titers. Luciferase signals and titers from lung homogenates of treated animals showed a significant reduction compared to levels of isotype control-treated animals (Fig. 5C and D). In fact, many treated animals did not show detectable virus titers (Fig. 5D). We saw a larger fold change in viral titers than in luciferase activity. This difference may be due to antibody-induced inhibition of the proteolytic ac-

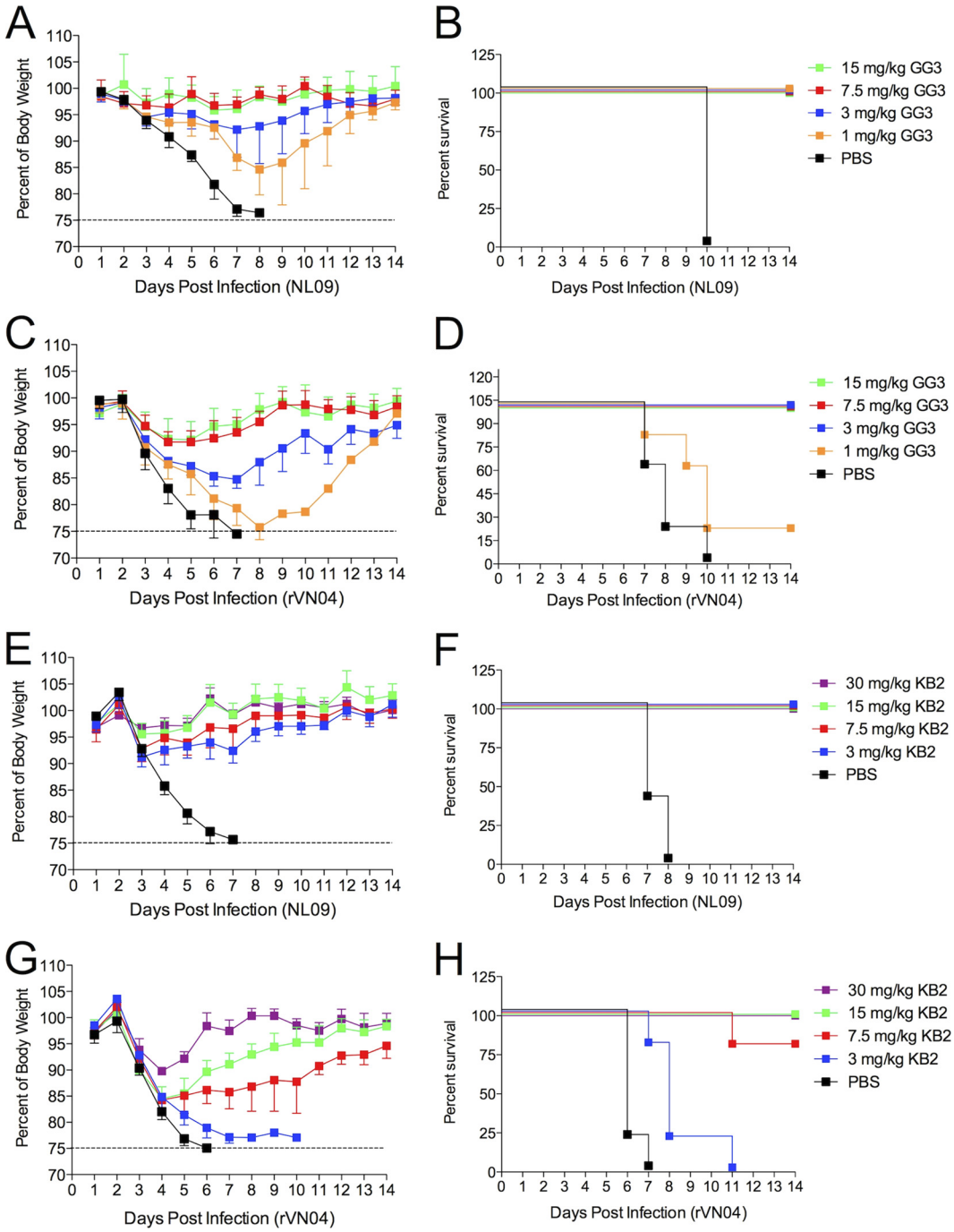

FIG 6 GG3 and KB2 protect BALB/c mice against lethal challenge with pandemic H1 and avian H5 influenza viruses. Mice were administered the indicated doses of antibody GG3 or KB2 and challenged with the pandemic H1N1 isolate NL09 (influenza A/Netherlands/602/2009) or the avian H5N1 isolate rVN04 (influenza A/Vietnam/1203/2004), as indicated. Weight loss and survival were monitored.

tivation of HA or inhibition of viral budding, as has been previously demonstrated for other cross-reactive anti-influenza virus antibodies (35, 36).

Imaging of the antibody treatment groups revealed a pronounced reduction in both the luciferase-positive area and signal strength compared to the controls (Fig. 5E). We next wanted to verify our PR8-GLuc results using viruses more relevant to human disease. Since BALB/c mice are a more standard genetic background for therapeutic efficacy studies, we repeated the animal challenge experiments in that background with two clinically relevant strains of IAV, a pandemic H1N1 isolate, influenza A/Netherlands/602/2009 (NL09) virus, and an H5N1 avian isolate, influenza A/Vietnam/1203/2004 (VN04) virus. As expected, pretreatment with GG3 and KB2 monoclonal antibodies led to protection from IAV disease with these viruses (Fig. 6A to H).

DISCUSSION

Influenza A virus infection poses a significant burden to human health. Novel tools and methods to monitor viral infection in living animals are needed to advance our current understanding of IAV pathogenesis and help to evaluate new therapeutic strategies. Studies of luciferase-expressing viruses *in vivo* are powerful tools that have already been used to interrogate pathogenesis strategies in both DNA and RNA viral systems such as the parainfluenza virus Sendai virus (37), Sindbis virus (38), human adenovirus (39), herpes simplex virus-1 (40, 41), vaccinia virus (42), dengue virus (43), and mouse coronavirus (44).

In this report we have developed a luciferase-expressing IAV and identified only the second site in the genome to tolerate a reporter gene insertion, the other reports being in the NS segment (32, 45). This virus was utilized to develop a method that allows noninvasive *in vivo* imaging with a segmented RNA virus. The virus, PR8-GLuc, was subsequently used to study the efficacy of monoclonal antibodies, which bind the conserved IAV hemagglutinin stalk and protect mice in challenge studies. Thus, we have described a new method for characterizing antiviral intervention strategies and provided a platform for additional pathogenesis studies.

Recently, an IAV with a rearranged genome, utilized for vaccine studies, was also reported to be capable of carrying luciferase (45). This virus, however, is designed to be safe for vaccination studies and, thus, is significantly attenuated in tissue culture and animals, which limits its utility for pathogenesis or therapeutic efficacy experiments. Our luciferase insertion, in contrast, was designed to minimize attenuation relative to the parental strain. Due to this, we observed only a 10-fold decrease in viral titers and an ~50- to 100-fold decrease in LD_{50} values. Additionally, our virus appears to be stable in serial passaging experiments and, in contrast to many previously described reporter viruses, retains the inserted reporter gene after passaging (25–29). PR8-GLuc has allowed for the development of a method for dynamic, whole-body imaging in which IAV infection and spread can be monitored in a noninvasive manner. This approach may be particularly useful as a metric in evaluating novel therapeutic agents and could significantly reduce the number of animals required for such studies since the mice can be monitored longitudinally.

We have used PR8-GLuc to characterize novel monoclonal antibodies that bind and neutralize virus of both the H5 and H1 subtypes. These antibodies provide protection from H1N1 and H5N1 viruses *in vivo*, providing additional evidence that cross-reactive antibodies that inhibit multiple subtypes of IAV are generated during influenza virus infection, and, importantly, can protect from disease. High-resolution scans of luciferase in the respiratory tract of multiple animal models may give insight into the contribution of tissue distribution to virus transmission and the eventual outcome of infection. These studies are particularly interesting in the context of central nervous system infection with highly pathogenic H5N1 viruses. And while the focus of this report has been on *in vivo* imaging of viral infection, the PR8-GLuc reporter virus has obvious potential for *in vitro* screening as well.

ACKNOWLEDGMENTS

This work was partially supported by NIH grant PO1 AI097092-01 and NIH contracts HHSN272200900032C and HHSN266200700010C. N.S.H. is supported by T32 AI07647-13.

We acknowledge Florian Krammer, Alita Kongchanagul, and Qinshan Gao for helpful discussions and reagent contribution and Jean Lim for critical reading of the manuscript.

N.S.H., V.H.L.-G., D.E., G.S.T., R.H., and P.P. designed experiments. N.S.H., V.H.L.-G., D.E., G.S.T., and R.H. performed experiments. N.S.H., V.H.L.-G., D.E., G.S.T., and P.P. analyzed data. N.S.H. and P.P. wrote the paper.

REFERENCES

1. **Palese P, Shaw ML.** 2007. *Orthomyxoviridae*: the viruses and their replication, p 1647–1689. *In* Knipe DM, Howley PM (ed), Fields virology, 5th ed. Lippincott Williams & Wilkins, Philadelphia, PA.
2. **Neumann G, Noda T, Kawaoka Y.** 2009. Emergence and pandemic potential of swine-origin H1N1 influenza virus. Nature **459:**931–939.
3. **Taubenberger JK, Morens DM.** 2008. The pathology of influenza virus infections. Annu. Rev. Pathol. **3:**499–522.
4. **Kuiken T, Riteau B, Fouchier RA, Rimmelzwaan GF.** 2012. Pathogenesis of influenza virus infections: the good, the bad and the ugly. Curr. Opin. Virol. **2:**276–286.
5. **Close DM, Xu T, Sayler GS, Ripp S.** 2011. In vivo bioluminescent imaging (BLI): noninvasive visualization and interrogation of biological processes in living animals. Sensors (Basel) **11:**180–206.
6. **Li H, Li JZ, Helm GA, Pan D.** 2007. Non-invasive imaging of firefly luciferase reporter gene expression using bioluminescence imaging in human prostate cancer models. Biotechnol. Appl. Biochem. **46:**179–184.
7. **Zabala M, Alzuguren P, Benavides C, Crettaz J, Gonzalez-Aseguinolaza G, Ortiz de Solorzano C, Gonzalez-Aparicio M, Kramer MG, Prieto J, Hernandez-Alcoceba R.** 2009. Evaluation of bioluminescent imaging for noninvasive monitoring of colorectal cancer progression in the liver and its response to immunogene therapy. Mol. Cancer **8:**2. doi:10.1186/1476-4598-8-2.
8. **Leevy WM, Serazin N, Smith BD.** 2007. Optical imaging of bacterial infection models. Drug Discov. Today Dis. Models **4:**91–97.
9. **Contag CH, Bachmann MH.** 2002. Advances in *in vivo* bioluminescence imaging of gene expression. Annu. Rev. Biomed. Eng. **4:**235–260.
10. **Rogers GN, Paulson JC.** 1983. Receptor determinants of human and animal influenza virus isolates: differences in receptor specificity of the H3 hemagglutinin based on species of origin. Virology **127:**361–373.
11. **Matrosovich M, Tuzikov A, Bovin N, Gambaryan A, Klimov A, Castrucci MR, Donatelli I, Kawaoka Y.** 2000. Early alterations of the receptor-binding properties of H1, H2, and H3 avian influenza virus hemagglutinins after their introduction into mammals. J. Virol. **74:**8502–8512.
12. **Zambon MC.** 2001. The pathogenesis of influenza in humans. Rev. Med. Virol. **11:**227–241.
13. **Jang H, Boltz D, Sturm-Ramirez K, Shepherd KR, Jiao Y, Webster R, Smeyne RJ.** 2009. Highly pathogenic H5N1 influenza virus can enter the central nervous system and induce neuroinflammation and neurodegeneration. Proc. Natl. Acad. Sci. U. S. A. **106:**14063–14068.
14. **Morishima T, Togashi T, Yokota S, Okuno Y, Miyazaki C, Tashiro M, Okabe N.** 2002. Encephalitis and encephalopathy associated with an influenza epidemic in Japan. Clin. Infect. Dis. **35:**512–517.
15. **Grimm D, Staeheli P, Hufbauer M, Koerner I, Martinez-Sobrido L, Solorzano A, Garcia-Sastre A, Haller O, Kochs G.** 2007. Replication fitness determines high virulence of influenza A virus in mice carrying functional Mx1 resistance gene. Proc. Natl. Acad. Sci. U. S. A. **104:**6806–6811.
16. **Gao Q, Palese P.** 2009. Rewiring the RNAs of influenza virus to prevent reassortment. Proc. Natl. Acad. Sci. U. S. A. **106:**15891–15896.
17. **Gao Q, Chou YY, Doganay S, Vafabakhsh R, Ha T, Palese P.** 2012. The influenza A virus PB2, PA, NP, and M segments play a pivotal role during genome packaging. J. Virol. **86:**7043–7051.
18. **Hai R, Krammer F, Tan GS, Pica N, Eggink D, Maamary J, Margine I, Albrecht RA, Palese P.** 2012. Influenza viruses expressing chimeric hemagglutinins: globular head and stalk domains derived from different subtypes. J. Virol. **86:**5774–5781.
19. **Bouvier NM, Lowen AC, Palese P.** 2008. Oseltamivir-resistant influenza A viruses are transmitted efficiently among guinea pigs by direct contact but not by aerosol. J. Virol. **82:**10052–10058.
20. **Tan GS, Krammer F, Eggink D, Kongchanagul A, Moran TM, Palese P.** 2012. A pan-H1 anti-hemagglutinin monoclonal antibody with potent broad-spectrum efficacy in vivo. J. Virol. **86:**6179–6188.
21. **Avilov SV, Moisy D, Munier S, Schraidt O, Naffakh N, Cusack S.** 2012. Replication-competent influenza A virus that encodes a split-green fluo-

rescent protein-tagged PB2 polymerase subunit allows live-cell imaging of the virus life cycle. J. Virol. **86:**1433–1448.
22. **Tannous BA, Kim DE, Fernandez JL, Weissleder R, Breakefield XO.** 2005. Codon-optimized Gaussia luciferase cDNA for mammalian gene expression in culture and in vivo. Mol. Ther. **11:**435–443.
23. **Ryan MD, Drew J.** 1994. Foot-and-mouth disease virus 2A oligopeptide mediated cleavage of an artificial polyprotein. EMBO J. **13:**928–933.
24. **Ellgaard L, Molinari M, Helenius A.** 1999. Setting the standards: quality control in the secretory pathway. Science **286:**1882–1888.
25. **Schoggins JW, Dorner M, Feulner M, Imanaka N, Murphy MY, Ploss A, Rice CM.** 2012. Dengue reporter viruses reveal viral dynamics in interferon receptor-deficient mice and sensitivity to interferon effectors in vitro. Proc. Natl. Acad. Sci. U. S. A. **109:**14610–14615.
26. **McGee CE, Shustov AV, Tsetsarkin K, Frolov IV, Mason PW, Vanlandingham DL, Higgs S.** 2010. Infection, dissemination, and transmission of a West Nile virus green fluorescent protein infectious clone by *Culex pipiens* quinquefasciatus mosquitoes. Vector Borne Zoonotic Dis. **10:**267–274.
27. **Pierson TC, Diamond MS, Ahmed AA, Valentine LE, Davis CW, Samuel MA, Hanna SL, Puffer BA, Doms RW.** 2005. An infectious West Nile virus that expresses a GFP reporter gene. Virology **334:**28–40.
28. **Tsetsarkin K, Higgs S, McGee CE, De Lamballerie X, Charrel RN, Vanlandingham DL.** 2006. Infectious clones of Chikungunya virus (La Reunion isolate) for vector competence studies. Vector Borne Zoonotic Dis. **6:**325–337.
29. **Agapov EV, Frolov I, Lindenbach BD, Pragai BM, Schlesinger S, Rice CM.** 1998. Noncytopathic Sindbis virus RNA vectors for heterologous gene expression. Proc. Natl. Acad. Sci. U. S. A. **95:**12989–12994.
30. **Pica N, Iyer A, Ramos I, Bouvier NM, Fernandez-Sesma A, Garcia-Sastre A, Lowen AC, Palese P, Steel J.** 2011. The DBA. 2 mouse is susceptible to disease following infection with a broad, but limited, range of influenza A and B viruses. J. Virol. **85:**12825–12829.
31. **Srivastava B, Blazejewska P, Hessmann M, Bruder D, Geffers R, Mauel S, Gruber AD, Schughart K.** 2009. Host genetic background strongly influences the response to influenza a virus infections. PLoS One **4:**e4857. doi:10.1371/journal.pone.0004857.
32. **Manicassamy B, Manicassamy S, Belicha-Villanueva A, Pisanelli G, Pulendran B, Garcia-Sastre A.** 2010. Analysis of in vivo dynamics of influenza virus infection in mice using a GFP reporter virus. Proc. Natl. Acad. Sci. U. S. A. **107:**11531–11536.
33. **Sui J, Hwang WC, Perez S, Wei G, Aird D, Chen LM, Santelli E, Stec B, Cadwell G, Ali M, Wan H, Murakami A, Yammanuru A, Han T, Cox NJ, Bankston LA, Donis RO, Liddington RC, Marasco WA.** 2009. Structural and functional bases for broad-spectrum neutralization of avian and human influenza A viruses. Nat. Struct. Mol. Biol. **16:**265–273.
34. **Wang TT, Tan GS, Hai R, Pica N, Petersen E, Moran TM, Palese P.** 2010. Broadly protective monoclonal antibodies against H3 influenza viruses following sequential immunization with different hemagglutinins. PLoS Pathog. **6:**e1000796. doi:10.1371/journal.ppat.1000796.
35. **Ekiert DC, Bhabha G, Elsliger MA, Friesen RH, Jongeneelen M, Throsby M, Goudsmit J, Wilson IA.** 2009. Antibody recognition of a highly conserved influenza virus epitope. Science **324:**246–251.
36. **Dreyfus C, Laursen NS, Kwaks T, Zuijdgeest D, Khayat R, Ekiert DC, Lee JH, Metlagel Z, Bujny MV, Jongeneelen M, van der Vlugt R, Lamrani M, Korse HJ, Geelen E, Sahin O, Sieuwerts M, Brakenhoff JP, Vogels R, Li OT, Poon LL, Peiris M, Koudstaal W, Ward AB, Wilson IA, Goudsmit J, Friesen RH.** 2012. Highly conserved protective epitopes on influenza B viruses. Science **337:**1343–1348.
37. **Burke CW, Mason JN, Surman SL, Jones BG, Dalloneau E, Hurwitz JL, Russell CJ.** 2011. Illumination of parainfluenza virus infection and transmission in living animals reveals a tissue-specific dichotomy. PLoS Pathog. **7:**e1002134. doi:10.1371/journal.ppat.1002134.
38. **Cook SH, Griffin DE.** 2003. Luciferase imaging of a neurotropic viral infection in intact animals. J. Virol. **77:**5333–5338.
39. **Hofherr SE, Shashkova EV, Weaver EA, Khare R, Barry MA.** 2008. Modification of adenoviral vectors with polyethylene glycol modulates in vivo tissue tropism and gene expression. Mol. Ther. **16:**1276–1282.
40. **Luker GD, Bardill JP, Prior JL, Pica CM, Piwnica-Worms D, Leib DA.** 2002. Noninvasive bioluminescence imaging of herpes simplex virus type 1 infection and therapy in living mice. J. Virol. **76:**12149–12161.
41. **Burgos JS, Guzman-Sanchez F, Sastre I, Fillat C, Valdivieso F.** 2006. Non-invasive bioluminescence imaging for monitoring herpes simplex virus type 1 hematogenous infection. Microbes Infect. **8:**1330–1338.
42. **Luker KE, Hutchens M, Schultz T, Pekosz A, Luker GD.** 2005. Bioluminescence imaging of vaccinia virus: effects of interferon on viral replication and spread. Virology **341:**284–300.
43. **Li XF, Deng YQ, Zhao H, Ye Q, Wang HJ, Li SH, Zhu SY, Shi PY, Qin ED, Zhang B, Qin CF.** 2013. Noninvasive bioluminescence imaging of dengue virus infection in the brain of A129 mice. Appl. Microbiol. Biotechnol. **97:**4589–4596.
44. **Raaben M, Prins HJ, Martens AC, Rottier PJ, De Haan CA.** 2009. Non-invasive imaging of mouse hepatitis coronavirus infection reveals determinants of viral replication and spread in vivo. Cell. Microbiol. **11:**825–841.
45. **Pena L, Sutton T, Chockalingam A, Kumar S, Angel M, Shao H, Chen H, Li W, Perez DR.** 2013. Influenza viruses with rearranged genomes as live-attenuated vaccines. J. Virol. **87:**5118–5127.